

Bright Monolayer Tungsten Disulfide *via* Exciton and Trion Chemical Modulations

Ye Tao,^{‡,a} Xuechao Yu,^{‡,a} Jiewei Li,^b Houkun Liang,^c Ying Zhang,^c Wei Huang^{b,d} and Qi Jie Wang^{*,a}

Received 00th January 20xx,
Accepted 00th January 20xx

DOI: 10.1039/x0xx00000x

www.rsc.org/

Atomically thin transition metal dichalcogenides (TMDCs) with exceptional electrical and optical properties have drawn tremendous attention for novel optoelectronic devices such as photodetectors, transistors and light emitters, etc. However, the electron bound trions formed through the combination of neutral exciton and electron significantly decrease the photoluminescence (PL) efficiency of TMDCs. In this study, we report a simple yet efficient chemical doping strategy to modulate the optical properties of monolayer tungsten disulfide (WS₂). As a demonstrative example, the chemical doped monolayer WS₂ exhibits remarkably PL enhancement, which is about one order of magnitude higher than pristine WS₂. This outstanding PL enhancement is attributed to the fact that the excess electron which promotes the formation of electron bound trions is effectively decreased through charge transfer from WS₂ to chemical dopant. Furthermore, an improved degree of circular polarization which is increased from ~9.0% to 41.5% is also observed in the chemical doped monolayer WS₂. Our work illustrates a feasible strategy to manipulate optical properties of TMDCs via exciton modulation, making TMDCs promising candidates for versatile semiconductor-based photonic devices.

Two-dimensional (2D) atomic layer materials have attracted exponential attention in diverse fields, not only for their fundamental scientific importance but also because of their

potential applications, ranging from electronics, photonics to valleytronics.¹⁻⁷ A typical example is the atomically thin transition metal dichalcogenides (TMDCs), a layered semiconductor consists of transition metal and chalcogenide atoms which are arranged in a hexagonal lattice.⁸⁻¹¹ It is well known that TMDCs possess layer dependent band gap and undergo a transition from an indirect band gap bulk crystals to direct band gap monolayer semiconductors. Monolayer TMDCs exhibit unique electrical properties and excellent optical performance, opening up conceptually novel optoelectronic devices, such as FETs, light emitting diodes, and photodetectors.¹²⁻¹⁵ Furthermore, monolayer TMDCs are ideal platform to investigate the valleytronics originated from the inversion symmetry breaking and spin-orbital coupling.^{13, 14} Commonly, the photo-excited hole and electron can form excitons on the basis of attractive Coulomb interaction. The excitons can further become electron bound trions through binding an additional electron owing to the natural n doping of the TMDCs.¹⁶ However, the formation of electron bound trion results in low photoluminescence quantum yield of monolayer TMDCs,^{16, 17} which has greatly obstructed their applications.¹⁸⁻²⁰ Therefore, the manipulation of electron bound trions concentration in monolayer TMDCs is of central importance for achieving high PL efficiency.

The regulation of electron density is demonstrated to be an effective strategy of tuning the neutral exciton and trion for achieving high PL efficiency in monolayer TMDCs.²⁰⁻²⁵ Electron density could be effectively changed through tuning gate voltage of FETs devices, resulting in significant exciton brightening in monolayer WS₂.^{21, 22} Four-fold PL efficiency enhancement in monolayer WS₂ through strong affinity fluorination plasma treatment was also reported.²⁰ The modulation of electron density in monolayer WS₂ also observed in WS₂/graphene vertical heterostructure through facilitating charge transfer from WS₂ to graphene, rendering efficient PL enhancement.²³ However, the electron density modulation realized by gate voltage tuning, gas physisorption, and vertical heterostructure requires complicated technological processes and precise control of the gas doping concentration and time to

^a Centre for OptoElectronics and Biophotonics, School of Electrical and Electronic Engineering & The Photonics Institute, Nanyang Technological University, 50 Nanyang Avenue, 639798, Singapore. E-mail: qjwang@ntu.edu.sg.

^b Key Laboratory of Flexible Electronics & Institute of Advanced Materials, Jiangsu National Synergetic Innovation Center for Advanced Materials, Nanjing Tech University, 30 South Puzhu Road, Nanjing 211816, China

^c Singapore Institute of Manufacturing Technology, 71 Nanyang Drive, 638075 Singapore

^d Key Laboratory for Organic Electronics and Information Displays & Institute of Advanced Materials, Jiangsu National Synergetic Innovation Center for Advanced Materials, Nanjing University of Posts & Telecommunications, 9 Wenyuan Road, Nanjing 210023, China

Electronic Supplementary Information (ESI) available: PL and Raman spectra before and after HATCN doping, rate equation and mass action law analysis, theoretical calculations analysis. See DOI: 10.1039/x0xx00000x

[‡]These authors contributed equally.

obtain the desired PL efficiency, leading to relatively high fabrication costs and limiting the fundamental study of monolayer WS_2 . As a result, it is imperative to develop a feasible and universal strategy to control electron density for tuning optoelectronic properties of monolayer WS_2 . Organic molecules

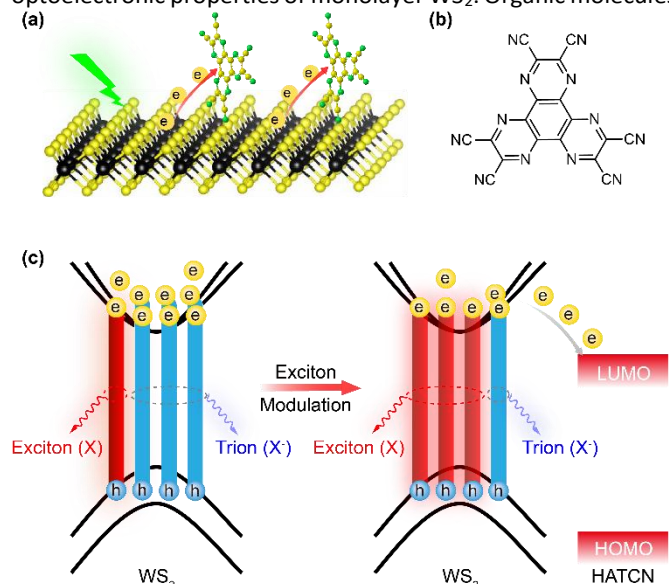


Fig. 1 Design concept and mechanism of exciton modulation for achieving bright monolayer WS_2 . (a) Schematic drawings of hexaazatriphenylenehexacarbonitrile (HATCN) doping in monolayer WS_2 . (b) Chemical structure of HATCN. (c) Schematic drawings of exciton modulation through chemical doping in WS_2 . The electron bond trions in the monolayer WS_2 can be effectively changed to the neutral excitons through charge transfer from the conduction band (CB) of WS_2 to the LUMO of HATCN.

doping *via* drop cast is well known as a promising method for tuning electron density in 2D materials.^{10, 18, 26–29} Nevertheless, there are few reports about robust PL enhancement in monolayer WS_2 based on organic molecule doping.¹⁹

HATCN (hexaazatriphenylenehexacarbonitrile) is a promising organic semiconductor which is widely used as the hole injection and buffer layer in the arena of organic light emitting diodes and organic solar cells owing to its strong electron withdrawing ability and deep highest occupied molecular orbital (HOMO) and lowest unoccupied molecular orbital (LUMO) energy level, making it a promising candidate for hybridizing with WS_2 to modulate the optoelectronic properties.^{30–33} In this work, we deposit HATCN solution onto monolayer WS_2 to modulate exciton and PL property of monolayer WS_2 (Fig. 1). The HATCN doped monolayer WS_2 successfully achieve a state-of-art PL enhancement, which is ~ 10 -fold higher than that from a pristine monolayer WS_2 . Additionally, we demonstrate that the HATCN doped monolayer WS_2 shows an increased degree of polarization (DOP), which increases from $\sim 9.0\%$ to 41.5% . In combination with the experimental and density functional theory (DFT) simulation results, we reveal that the electron density significantly decreases in monolayer WS_2 through charge transfer from monolayer WS_2 to HATCN (Fig. 1), which promotes the transition from electron bound trions to neutral excitons and decreases the intervalley scattering. This renders the enhancement of PL intensity and DOP in monolayer WS_2 .

The monolayer WS_2 flake was conveniently exfoliated from the bulk crystals by a standard micromechanical method, followed by transferring onto a Si wafer with a 280 nm thick SiO_2 coated layer.³⁴ To reveal the exact layer number of WS_2 flakes, the exfoliated sample was investigated by optical microscopy (OM),

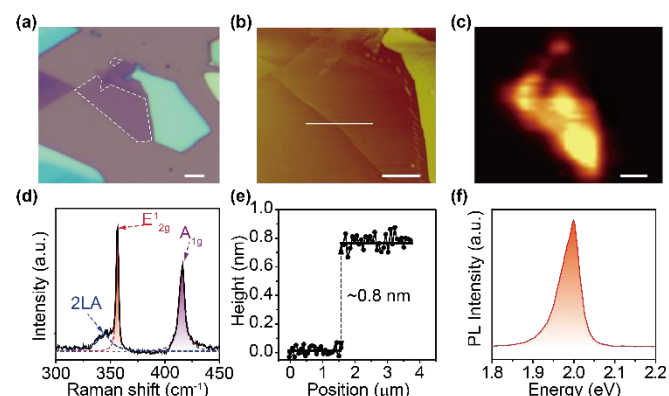


Fig. 2 Preparation and characterization of monolayer WS_2 . (a) Optical image, (b) AFM image (c) PL mapping and (d) Raman spectrum of a WS_2 flake on SiO_2/Si substrate measured at room temperature. (e) The AFM height measured along the line in (b). (f) The PL spectrum extracted from PL mapping (c). The scale bar in (a), (b) and (c) is $2 \mu\text{m}$.

atomic force microscopy (AFM), Raman spectrum and PL measurement. The typical optical image of monolayer WS_2 flake is shown in Fig. 2a and then the thickness was measured to be ~ 0.8 nm through AFM with non-contact mode (Fig. 2b,e). The Raman spectrum (Fig. 2d) excited with a 488 nm laser shows a strong out of plane A_{1g} peak at $\sim 417 \text{ cm}^{-1}$ and an intense combinational Raman peak consisting of 2LA peak at $\sim 350 \text{ cm}^{-1}$ and in-plane E_{2g}^1 peak at $\sim 355 \text{ cm}^{-1}$.¹⁸ The frequency difference between E_{2g}^1 and A_{1g} peak is $\sim 62.3 \text{ cm}^{-1}$, which unambiguously confirms that the flake is a monolayer WS_2 .³⁵ The PL spectra measured by a micro-PL system is also used to reveal the exact number of WS_2 flake. The PL mapping (Fig. 2c) exhibits a bright emission for the monolayer WS_2 , while the emission is quite weak for the few layer WS_2 . The different PL intense between monolayer and few-layer WS_2 is due to the transition from direct to indirect band gap.¹⁹ The non-uniformity intensity of the PL mapping may be due to the variation of natural doping (n doping) in the pristine monolayer WS_2 , as relatively high trion contributions (low energy PL shoulder) in area with weak PL intensity are observed (Figure S2).³⁶ The PL spectrum extracted from the mapping shows a peak at $\sim 1.99 \text{ eV}$ (Fig. 2f) for the monolayer WS_2 . It should be noted that the B exciton is not detectable under this laser excitation (532 nm) owing to the energy difference which arises from strong spin-orbit interaction is as large as 0.4 eV between A and B exciton.³⁷ To test the feasibility of exciton modulation through the chemical doping, the PL spectra of pristine and HATCN doped monolayer WS_2 were systematically investigated (Fig. 3). The pristine monolayer WS_2 shows a wide PL spectrum with an emission peak at $\sim 1.99 \text{ eV}$ (Fig. 3a), which is the emission from both neutral exciton (X) and electron bound trion (X⁻) states owing to the heavily n-doped of pristine monolayer WS_2 .³⁶ In contrast, the PL intensity of monolayer WS_2 undergoes apparent variation after the HATCN doping. It should be noted

that the PL intensities are dramatically enhanced with the increase of the doping steps and become saturated after 6 times doping process. The PL intensity of HATCN doped monolayer WS₂ is more than ~10 fold that of pristine monolayer WS₂, which is among the best results of PL enhancement reported to date (Table S1). On the other hand, the PL spectra become sharp and blue shift with an emission peak at ~2.02 eV after the HATCN doping and can be clearly fitted with two peaks (X⁻ and X) using

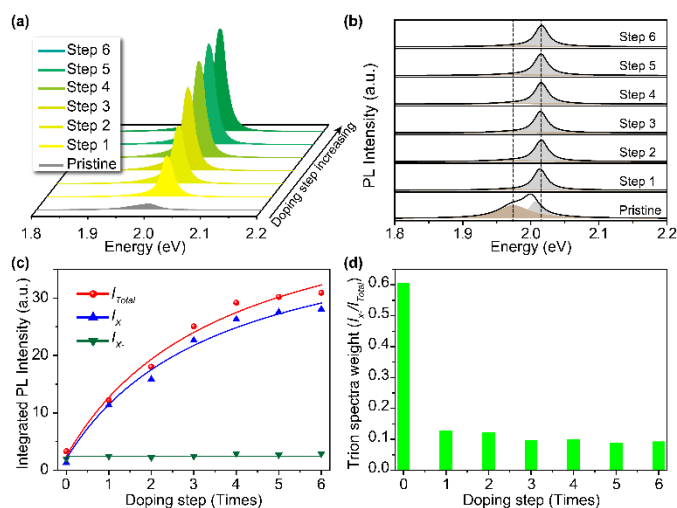


Fig. 3 PL variation of monolayer WS₂ before and after HATCN doping. (a) The PL spectra of monolayer WS₂ measured at different HATCN doping step from 0 to 6. (b) The evolution of PL spectra of monolayer WS₂ as the HATCN doping step increases. Note that the PL spectra are fitted through the Lorentzian fitting, which are assigned to the trion (X⁻) and neutral exciton (X). (c) The integrated PL intensity of trion (I_{X^-}), neutral exciton (I_X) and the sum (I_{total}) of I_{X^-} and I_X as a function of HATCN doping step. The discrete points are the experimental results, while the solid lines are theoretical results fitted through rate equation. (d) The trion spectra weight (I_{X^-}/I_{total}) as a function of HATCN doping step.

Lorentzian function (Fig. 3b and S1). In order to figure out the spectral weight of each component, the integrated PL intensity of trion, neutral exciton, and total intensity was evaluated according to the Lorentzian fitting results.²⁸ As shown in Fig. 3c,d, the intensity of trion is predominant and trion spectra weight is as high as ~0.6 in the pristine monolayer WS₂. However, the intensity of trion is drastically decreased and the trion spectra weight is as low as ~0.1 after 6 times doping process, indicating that the neutral exciton becomes predominant because of transition from trions (X⁻) to neutral excitons (X) in monolayer WS₂ after the HATCN doping. In order to gain insight into the PL intensity variation in HATCN doped WS₂, the excited dynamics in monolayer WS₂ was discussed based on a three-level model (Fig. 4a).²⁷ According to the rate equation, the PL intensity of neutral exciton (I_X) and trion (I_{X^-}) can be expressed as follows (see Supporting Information):²⁸

$$I_X(n) = \frac{AG\gamma_{ex}}{\Gamma_{ex} + k_r(n)} \quad (1)$$

$$I_{X^-}(n) = \frac{k_r(n)}{\Gamma_{tr}} \frac{AG\gamma_{tr}}{\Gamma_{ex} + k_r(n)} \quad (2)$$

where A is coefficient, γ_{ex} and γ_{tr} are the radiative decay rate of the neutral exciton (I_X) and trion (I_{X^-}), respectively. In order to simplify the analysis, the variation of γ_{ex} and γ_{tr} are neglected with the doping step increases. The experimental PL intensity of trion (I_{X^-}) and neutral exciton (I_X) can be fitted by equation (1) and (2), as shown in Fig. 3c (solid line). The best fitting result of γ_{tr}/γ_{ex} is 0.06, which demonstrate that the radiative rate of trion is significantly lower than that of neutral excitons, suggesting enhanced PL emission from the neutral excitons.

Under the assumption that the mass action law is valid, the relationship among the population of neutral excitons, trions

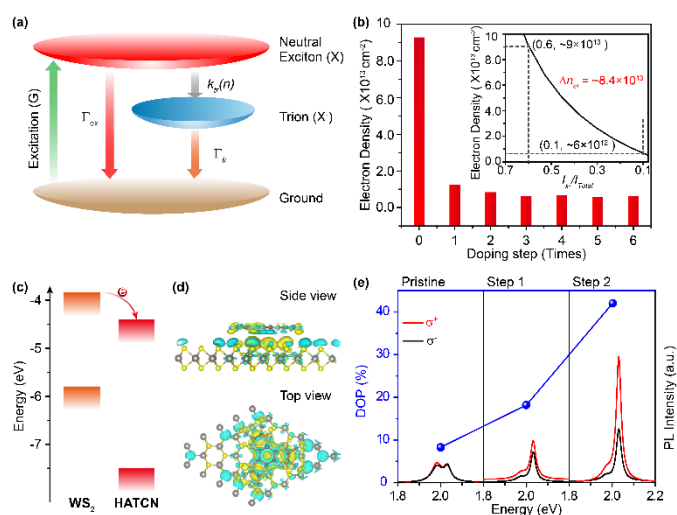


Fig. 4 Exciton analysis and theoretical calculation of chemical doped WS₂. (a) Schematic drawing of the three energy level model, G is the population of excitons after optical excitation, $k_r(n)$ is the generation rate of the trion (X) from the neutral exciton (X) after n -th doping step, Γ_{ex} and Γ_{tr} are the decay rate of neutral exciton and trion, respectively. (b) The experimental electron density as a function of HATCN doping step. The inset is calculated electron density based on mass action law model. (c) Energy level of WS₂ and HATCN and schematic drawing of the charge transfer from the CB of WS₂ to the LUMO of HATCN. (d) The calculated electron density difference before and after HATCN doping. The yellow and cyan color represent the accumulation and depletion of the electron. (e) The circularly polarized PL spectra and DOP of pristine and HATCN doped WS₂. The DOP can be expressed as $P = (I_+ - I_-)/(I_+ + I_-)$, where the I_+ and I_- are the intensity of the right (δ^+) and left (δ^-) hand PL emission, respectively.

and electron density in monolayer WS₂ can be expressed as^{19, 38}

$$\frac{N_X n_{el}}{N_{X^-}} = \left(\frac{4m_X m_e}{\pi \hbar^2 m_{X^-}} \right) k_B T \exp \left(\frac{E_b}{k_B T} \right) \quad (3)$$

where \hbar is the reduced Planck's constant, k_B is the Boltzmann constant, T is the temperature, E_b (~25 meV) is the trion binding energy, m_e , m_{X^-} and m_X are electron, trion and neutral exciton effective masses, respectively. m_e and m_h are $0.44m_0$ and $0.45m_0$, where m_0 is a free electron mass.³⁹ The effective mass of a neutral exciton (m_X) and a trion (m_{X^-}) can be calculated as $m_X = m_e + m_h = 0.89m_0$, $m_{X^-} = 2m_e + m_h = 1.34m_0$, respectively.²⁰ Therefore, the trion PL weight (I_{X^-}/I_{total}) can be determined as (see Supporting Information)

$$\frac{I_{X^-}}{I_{total}} = \frac{\gamma_{tr} N_{X^-}}{1 + \frac{\gamma_{tr} N_{X^-}}{\gamma_{ex} N_X}} \approx \frac{1.65 \times 10^{-14} n_{el}}{1 + 1.65 \times 10^{-14} n_{el}} \quad (4)$$

Thus, the calculated electron density n_{el} can be estimated from the trion spectra weight (I_X/I_X , Fig. 4b inset) by the equation (4). The experimental electron density is illustrated in Fig. 4b. The electron density in pristine monolayer WS₂ is $\sim 9 \times 10^{13} \text{ cm}^{-2}$ owing to its heavily n-doped characteristic, while the electron density sharply decreases to $\sim 8 \times 10^{12} \text{ cm}^{-2}$ after 2 times doping and becomes constant ($\sim 6 \times 10^{12} \text{ cm}^{-2}$) after 4 times doping. It is worthy to note that the variation of electron density (Δn_{el}) before and after HATCN doping is simulated as high as $\sim 8.4 \times 10^{13} \text{ cm}^{-2}$. These results indicate that the HATCN doping can effectively regulate the electron density in monolayer WS₂, which could be an effective way to manipulate the optical and electrical properties of WS₂.

The origin of PL modulation through HATCN doping can be regarded as charge transfer from monolayer WS₂ to the HATCN. The energy level of monolayer WS₂ and HATCN is illustrated in Fig. 4c, revealing that HATCN forms a type II *p-n* heterojunction with monolayer WS₂. The lower LUMO level of HATCN than the CB of monolayer WS₂ leads to significantly accumulated electrons on HATCN owing to the free electrons locate the bottom of conduction band of WS₂, thus reducing the formation probability of electron bound trion.

To further understand the PL enhancement of HATCN doped monolayer WS₂, we conducted first-principles calculations using the GGA/PBE⁴⁰ method with Tkatchenko–Scheffler dispersion correction⁴¹ in Material Studio2017 Castep module⁴². The commonly used dopant, 2,3,5,6-tetrafluoro-7,7,8,8-tetracyanoquinodimethane (F₄TCNQ), was also calculated for comparison.^{19, 28} According to the theoretical calculations, HATCN withdraws about 0.18 e charges from the WS₂ layer (Mulliken population analysis),⁴³ which is two times larger than that of F₄TCNQ (~ 0.09 e). With a consideration of its strong electron withdrawing ability, HATCN doped WS₂ showed higher PL enhancement than that of F₄TCNQ doped WS₂ (Table S2). In order to gain a direct insight into the decrease of electron density in monolayer WS₂, the calculated charge density difference before and after HATCN doping was mapped out by subtracting the electron of HATCN doped WS₂ from that of isolated components of WS₂ and HATCN. As shown in Fig. 4d, the charge density is redistribution and accumulates at the HATCN and interface of HATCN and WS₂ junction. It should be noted that the absorption energy of HATCN is -1.93 eV (Table S2), which is slight higher than that of F₄TCNQ, demonstrating the physical adsorption of HATCN on monolayer WS₂.^{19, 44}

Light-emitting from K and K' valleys of TMDCs shows opposite circular polarization light (right and left hand) owing to the breaking inversion symmetry, which has been widely investigated in opto-valleytronics.^{13, 45, 46} The modulation of electron density is also an effective way to tune the DOP of TMDCs.^{14, 27} Given the simple modulation of electron density in WS₂ through chemical doping, we further investigated the variation of DOP in WS₂ before and after chemical doping. As shown in Fig. 4e, the PL intensity of the right (δ^+) and left (δ^-) hand emission in HATCN doped WS₂ is significantly enhanced with the increase of doping steps, which is in accordance with the normal PL emission, indicating the decrease of the electron density. More importantly, the DOP also increases in HATCN

doped WS₂. The DOP of pristine WS₂ is $\sim 9.0\%$, while it increases to $\sim 18\%$ after one-step doping and to $\sim 41.5\%$ after two-step doping. The increase of the DOP in HATCN doped WS₂ may attribute to the decreasing of K \leftrightarrow K' intervalley scattering triggered by the decreasing of electron density.^{12, 20, 23}

Conclusions

In summary, we have proposed an efficient exciton modulation approach, *p*-type HATCN doping on monolayer WS₂ via drop cast, for tuning the optical properties of WS₂. The chemical doped monolayer WS₂ exhibits remarkably PL enhancement up to ~ 10 fold. Our results demonstrate that the modulation of electron density through charge transfer from *n*-doped WS₂ to HATCN is the key to modulate excitons in monolayer WS₂ for achieving high PL efficiency. The decrease of electron density leads to the trions to neutral excitons transition. Furthermore, benefitting from the flexibility in manipulating of the electron density through chemical doping, the HATCN doped monolayer WS₂ also show a tunable degree of circular polarization, which is increased from $\sim 9.0\%$ to 41.5%. This work not only develops a method to achieve bright monolayer TMDCs but also opens a new avenue for improving the degree of circular polarization.

Conflicts of interest

The authors declare no conflict of interests.

Acknowledgements

SERC (Grant No. 1426500050) from the Agency for Science, Technology and Research (A*STAR), Singapore National Research Foundation, Competitive Research Program (NRF-CRP16-2015-03), Singapore Ministry of Education Tier 2 Program (MOE2016-T2-1-128), National Natural Science Foundation of China (61704082) and Natural Science Foundation of Jiangsu Province (BK20170851) and Jiangsu Planned Projects for Postdoctoral Research Funds (1601031A).

Notes and references

- L. J. Li, E. O'Farrell, K. P. Loh, G. Eda, B. Ozyilmaz and A. Neto, *Nature*, 2016, **529**, 129-185.
- M. Amani, D. H. Lien, D. Kiriya, J. Xiao, A. Azcatl, J. Noh, S. R. Madhupathy, R. Addou, S. KC, M. Dubey, K. Cho, R. M. Wallace, S. C. Lee, J. H. He, J. W. Ager, X. Zhang, E. Yablonovitch and A. Javey, *Science*, 2015, **350**, 1065-1068.
- Z. Wang, Z. Dong, Y. Gu, Y. Chang, L. Zhang, L. Li, W. Zhao, G. Eda, W. Zhang, G. Grinblat, S. A. Maier, J. K. W. Yang, C. Qiu and A. T. S. Wee, *Nat. Commun.*, 2016, **7**, 11283.
- M. Wang, W. Li, L. Scarabelli, B. B. Rajeeva, M. Terrones, L. M. Liz-Marzán, D. Akinwande and Y. Zheng, *Nanoscale*, 2017, **9**, 13947-13955.
- X. Huang, C. L. Tan, Z. Y. Yin and H. Zhang, *Adv. Mater.*, 2014, **26**, 2185-2204.
- S. Zhang, S. Guo, Z. Chen, Y. Wang, H. Gao, J. Gómez-Herrero, P. Ares, F. Zamora, Z. Zhu and H. Zeng, *Chem. Soc. Rev.*, 2018, **47**, 982-1021.

- 7 S. C. Dhanabalan, J. S. Ponraj, H. Zhang and Q. Bao, *Nanoscale*, 2016, **8**, 6410-6434.
- 8 C. Tan, X. Cao, X. Wu, Q. He, J. Yang, X. Zhang, J. Chen, W. Zhao, S. Han, G. Nam, M. Sindoro and H. Zhang, *Chem. Rev.*, 2017, **117**, 6225-6331.
- 9 X. Duan, C. Wang, A. Pan, R. Yu and X. Duan, *Chem. Soc. Rev.*, 2015, **44**, 8859-8876.
- 10 H. T. Wang, H. T. Yuan, S. S. Hong, Y. B. Li and Y. Cui, *Chem. Soc. Rev.*, 2015, **44**, 2664-2680.
- 11 C. L. Tan and H. Zhang, *Chem. Soc. Rev.*, 2015, **44**, 2713-2731.
- 12 Y. Cui, R. Xin, Z. H. Yu, Y. M. Pan, Z. Y. Ong, X. X. Wei, J. Z. Wang, H. Y. Nan, Z. H. Ni, Y. Wu, T. S. Chen, Y. Shi, B. G. Wang, G. Zhang, Y. W. Zhang and X. R. Wang, *Adv. Mater.*, 2015, **27**, 5230-5234.
- 13 Y. Ye, J. Xiao, H. Wang, Z. Ye, H. Zhu, M. Zhao, Y. Wang, J. Zhao, X. Yin and X. Zhang, *Nat. Nanotechnol.*, 2016, **11**, 598-602.
- 14 W. Yang, J. Shang, J. Wang, X. Shen, B. Cao, N. Peimyoo, C. Zou, Y. Chen, Y. Wang, C. Cong, W. Huang and T. Yu, *Nano Lett.*, 2016, **16**, 1560-1567.
- 15 X. Yu, Z. Dong, Y. Liu, T. Liu, J. Tao, Y. Zeng, J. K. W. Yang and Q. J. Wang, *Nanoscale*, 2016, **8**, 327-332.
- 16 J. S. Ross, S. Wu, H. Yu, N. J. Ghimire, A. M. Jones, G. Aivazian, J. Yan, D. G. Mandrus, D. Xiao, W. Yao and X. Xu, *Nat. Commun.*, 2013, **4**, 1474.
- 17 K. F. Mak, K. He, C. Lee, G. H. Lee, J. Hone, T. F. Heinz and J. Shan, *Nat. Mater.*, 2012, **12**, 207-211.
- 18 C. R. Ryder, J. D. Wood, S. A. Wells and M. C. Hersam, *ACS Nano*, 2016, **10**, 3900-3917.
- 19 N. Peimyoo, W. Yang, J. Shang, X. Shen, Y. Wang and T. Yu, *ACS Nano*, 2014, **8**, 11320-11329.
- 20 Y. I. Jhon, Y. Kim, J. Park, J. H. Kim, T. Lee, M. Seo and Y. M. Jhon, *Adv. Funct. Mater.*, 2016, **26**, 7551-7559.
- 21 B. Zhu, X. Chen and X. Cui, *Sci. Rep.-UK*, 2015, **5**, 9218.
- 22 B. Zhu, H. Zeng, J. Dai, Z. Gong and X. Cui, *P. Natl. Acad. Sci. Usa.*, 2014, **111**, 11606-11611.
- 23 C. E. Giusca, I. Rungger, V. Panchal, C. Melios, Z. Lin, Y. Lin, E. Kahn, A. L. Elías, J. A. Robinson, M. Terrones and O. Kazakova, *ACS Nano*, 2016, **10**, 7840-7846.
- 24 K. P. Dhakal, S. Roy, S. J. Yun, G. Ghimire, C. Seo and J. Kim, *J. Mater. Chem. C.*, 2017, **5**, 6820-6827.
- 25 J. Choi, H. Zhang and J. H. Choi, *ACS Nano*, 2015, **10**, 1671-1680.
- 26 A. Tarasov, S. Zhang, M. Tsai, P. M. Campbell, S. Graham, S. Barlow, S. R. Marder and E. M. Vogel, *Adv. Mater.*, 2015, **27**, 1175-1181.
- 27 Z. Li, R. Ye, R. Feng, Y. Kang, X. Zhu, J. M. Tour and Z. Fang, *Adv. Mater.*, 2015, **27**, 5235-5240.
- 28 S. Mouri, Y. Miyauchi and K. Matsuda, *Nano Lett.*, 2013, **13**, 5944-5948.
- 29 X. Zhang, Z. Shao, X. Zhang, Y. He and J. Jie, *Adv. Mater.*, 2016, **28**, 10409-10442.
- 30 K. Udagawa, H. Sasabe, C. Cai and J. Kido, *Adv. Mater.*, 2014, **26**, 5062-5066.
- 31 J. L. Segura, R. Juárez, M. Ramos and C. Seoane, *Chem. Soc. Rev.*, 2015, **44**, 6850-6885.
- 32 Y. Tao, K. Yuan, T. Chen, P. Xu, H. Li, R. Chen, C. Zheng, L. Zhang and W. Huang, *Adv. Mater.*, 2014, **26**, 7931-7958.
- 33 Y. Ma, Y. Chung, L. Zheng, D. Zhang, X. Yu, L. Xiao, Z. Chen, S. Wang, B. Qu, Q. Gong and D. Zou, *ACS Appl. Mater. Inter.*, 2015, **7**, 6406-6411.
- 34 X. Yu, S. Zhang, H. Zeng and Q. J. Wang, *Nano Energy*, 2016, **25**, 34-41.
- 35 W. Zhao, Z. Ghorannevis, K. K. Amara, J. R. Pang, M. Toh, X. Zhang, C. Kloc, P. H. Tan and G. Eda, *Nanoscale*, 2013, **5**, 9677-9683.
- 36 P. K. Chow, R. B. Jacobs-Gedrim, J. Gao, T. Lu, B. Yu, H. Terrones and N. Koratkar, *ACS Nano*, 2015, **9**, 1520-1527.
- 37 B. Zhu, H. Zeng, J. Dai and X. Cui, *Adv. Mater.*, 2014, **26**, 5504-5507.
- 38 J. Siviniant, D. Scalbert, A. V. Kavokin, D. Coquillat and J. P. Lascaray, *Phys. Rev. B*, 1999, **59**, 1602-1604.
- 39 A. Ramasubramaniam, *Phys. Rev. B*, 2012, **86**, 115409.
- 40 J. P. Perdew, K. Burke and M. Ernzerhof, *Phys. Rev. Lett.*, 1996, **77**, 3865-3868.
- 41 M. Scheffler and A. Tkatchenko, *Phys. Rev. Lett.*, 2009, **102**, 73005.
- 42 S. J. Clark, M. D. Segall, C. J. Pickard, P. J. Hasnip, M. J. Probert, K. Refson and M. C. Payne, *Kristallogr.*, 2005, **220**, 567-570.
- 43 J. Li, Y. Liu, L. Xie, J. Shang, Y. Qian, M. Yi, T. Yu and W. Huang, *Phys. Chem. Chem. Phys.*, 2015, **17**, 4919-4925.
- 44 L. Chen, L. Wang, Z. Shuai and D. Beljonne, *J. Phys. Chem. Lett.*, 2013, **4**, 2158-2165.
- 45 H. Su, C. Wei, A. Deng, D. Deng, C. Yang and J. Dai, *Nanoscale*, 2017, **9**, 5148-5154.
- 46 Z. Sun, J. Gu, A. Ghazaryan, Z. Shotan, C. R. Consideine, M. Dollar, B. Chakraborty, X. Liu, P. Ghaemi, S. Kéna-Cohen and V. M. Menon, *Nat. Photonics*, 2017, **11**, 491-496.